Mathematical Biosciences and Engineering

MBE, 22 (9): 2409–2433.
DOI: 10.3934/mbe.2025088
Received: 07 April 2025
Revised: 28 May 2025
Accepted: 20 June 2025
Published: 22 July 2025

https://www.aimspress.com/journal/MBE

Research article

Multivariable optimal control for hemodialysis: A physiologically-grounded simulation study

Redemtus Heru Tjahjana[1,*], Ratna Herdiana[1], Zani Anjani Rafsanjani HSM[1] and Yogi Ahmad Erlangga[2]

[1] Department of Mathematics, Faculty of Science and Mathematics, Diponegoro University, Indonesia
[2] Department of Mathematics, College of Health and Natural Sciences, Zayed University, Abu Dhabi United Arab Emirates

*** Correspondence:** Email: redemtusherutjahjana@lecturer.undip.ac.id.

Abstract: This study introduces a novel multivariable optimal control framework for hemodialysis, which uniquely integrates five physiological states (blood urea concentration, fluid volume, blood pressure, electrolytes, and hemoglobin) with three clinically adjustable inputs (ultrafiltration rate, blood flow, and dialysate composition). By employing the limited-memory Broyden-Fletcher-Goldfarb-Shanno-B (L-BFGS-B) algorithm with patient-specific box constraints, the model enforces patient-specific physiological safety limits while dynamically balancing clinical targets. Numerical simulations demonstrate the stabilization of key parameters within ±5% of clinical benchmarks (e.g., KDIGO guidelines), though deviations in the hemodynamic responses underscore the need for adaptive control in real-world scenarios. Urea clearance trajectories align with efficacy patterns observed in practice, while blood pressure fluctuations reveal systematic offsets that require protocol refinement. This work bridges control theory with hemodialysis dynamics, thus offering a simulation-driven foundation for future clinical validation and personalized treatment optimization.

Keywords: optimal control; hemodialysis modeling; physiological variables; L-BFGS-B algorithm; personalized treatment

1. Introduction

Hemodialysis remains a cornerstone therapy for end-stage renal disease (ESRD), with

mathematical modeling playing an increasingly critical role in treatment optimization [1–3]. Early foundational studies focused on isolated physiological parameters, such as urea kinetics [4] and fluid balance [5], while subsequent work expanded to incorporate blood pressure dynamics [6], electrolyte transport [7], and hemoglobin synthesis [8]. Recent advancements span diverse methodologies, including dynamic optimization for personalized dialysis scheduling [9], machine learning approaches for chronic kidney disease prediction [10], and patient-centered models that address vascular access preferences [11] and acid-base balance [12]. Despite these innovations, critical gaps persist in the literature.

A key limitation lies in the predominant focus on isolated parameters, exemplified by urea-centric models [13] and sodium-profiling studies [14], which overlook the complex interplay of physiological variables during hemodialysis. While prior studies have optimized isolated parameters (e.g., urea kinetics [4], and hemodynamics [6]), the integration of multiple interdependent variables—blood urea, fluid volume, blood pressure, electrolytes, and hemoglobin—into a unified control framework remains underexplored. This gap limits the development of holistic protocols that address clinical complexity. Furthermore, while adaptive control strategies [15] and stochastic frameworks [16] have emerged, few enforce clinically actionable safety constraints, such as ultrafiltration rate limits [17] and hemoglobin stability thresholds [18]. Compounding these issues is the frequent lack of rigorous validation against either heterogeneous clinical datasets [19] or patient-reported outcomes [20], thus limiting the translational relevance [21].

To address these gaps, we propose a novel multivariable control framework that integrates five interdependent physiological variables into a unified ordinary differential equation (ODE) system. By implementing physiological box constraints via the limited-memory Broyden-Fletcher-Goldfarb-Shanno-B (L-BFGS-B) algorithm, our model adheres to clinical safety thresholds (e.g., ultrafiltration rates <1.3 mL/kg/h [17]) while enabling patient-specific protocol adjustments through customizable cost functionals. Although validated against idealized clinical benchmarks (Table 2), we explicitly acknowledge the limitations in generalizability, thus paving the way for future adaptations using heterogeneous patient data [19,20].

This work bridges the divide between theoretical control models and clinical hemodialysis practices, thus offering a pathway toward individualized ESRD management that harmonizes computational rigor with clinical pragmatism [21,22]. A comparative analysis of key hemodialysis models underscores the distinct contributions of our framework (Table 1). While prior works focused on subsets of variables (e.g., urea/fluid in Bachhiesl et al. [3], and sodium/fluid in Coli et al. [5]), our model integrates five interdependent physiological states—blood urea, fluid volume, blood pressure, electrolytes, and hemoglobin—to enable holistic control. Unlike prior models that optimize isolated parameters (e.g., urea kinetics in [4], hemodynamics in [6], and electrolyte balance in [5]), our approach explicitly accounts for interdependencies between these variables, thus offering a clinically nuanced solution that addresses the multifactorial nature of hemodialysis. Unlike static dialysate protocols (Pietribiasi et al. [14]) or single-variable optimizations (Rogg et al. [17]), our approach dynamically coordinates ultrafiltration (u_1), blood flow (u_2), and dialysate composition (u_3) via the L-BFGS-B algorithm, thus ensuring a real-time adaptation to physiological targets.

Recent advancements in multivariable dialysis optimization underscore the need for integrated frameworks. For instance, Sammarchi et al. [19] demonstrated the potential of machine learning in predicting and managing chronic kidney disease, thus emphasizing the model interpretability for clinical translation. Similarly, Guimaraes et al. [6] highlighted the superiority of hemodiafiltration over conventional hemodialysis in meta-analyses, thus reinforcing the importance of dynamic control

strategies. Building on these insights, our work extends the mathematical modeling paradigm by incorporating five interdependent physiological states, thus addressing gaps identified in recent multivariable analyses.

Table 1. Comparative analysis of hemodialysis optimization models.

Study	Variables Modeled	Control Strategy	Novelty of Our Work
Bachhiesl et al. [3]	Urea, Fluid Volume	Gradient-based optimization	5 variables (includes BP, electrolytes, Hb) + L-BFGS-B
Coli et al. [5]	Sodium, Fluid Balance	Profiled sodium dialysis	Dynamic electrolyte control via $u_3(t)$
Pietribiasi et al. [14]	Acid-base transport	Static dialysate composition	Real-time $u_3(t)$ optimization
Rogg et al. [17]	Urea, Hemoglobin (EPO)	EPO dosing only	Integrated hemodynamic control (u_1,u_2,u_3) + L-BFGS-B

A mathematical model is proposed to describe the hemodialysis dynamics, which is governed by a system of ODEs with constant coefficients. The framework integrates five physiological states—blood urea concentration (BUC), fluid volume, blood pressure, electrolytes, and hemoglobin—alongside three control inputs: ultrafiltration rate (UFR), blood flow rate, and dialysate composition. The cost functional J quantifies deviations from clinical targets and control effort, thus enabling the identification of protocols that minimize physiological imbalances while maintaining homeostasis.

The objectives of this study are threefold: (1) to develop a mathematical framework that captures hemodialysis dynamics through physiological state variables and control inputs; (2) to investigate the impact of the ultrafiltration rate, blood flow, and dialysate composition on the treatment efficacy; and (3) to identify optimal protocols via numerical simulations using the L-BFGS-B algorithm. These aims collectively advance personalized hemodialysis optimization while balancing clinical feasibility and patient safety. The proposed framework is operationalized through the following methodology, thereby combining dynamical modeling and numerical optimization.

2. Methods

Here are the steps of research methodology.

2.1. Formulation of mathematical model

The first step involves formulating a mathematical model to describe the dynamics of hemodialysis. The model is represented by a system of ODEs with constant coefficients, thus capturing the relationships between the state variables $(x_1 - x_5)$ that represent the BUC, fluid volume, blood pressure, electrolyte levels, and hemoglobin levels, and the control variables (u_1, u_2, and u_3) that represent the UFR, blood flow rate, and dialysate composition.

2.2. Optimal control approach

The study employs an optimal control approach to optimize the hemodialysis protocols. The objective of optimal control is to determine control policies that minimize a cost functional *J*, which is an integral of the squared deviations between the state variables and their target values, as well as the squared control inputs over a specified time horizon.

2.3. Solution of differential equations

The system of differential equations derived from the mathematical model is solved using appropriate numerical solution techniques, such as Runge-Kutta methods, to obtain numerical solutions for the state variables as functions of time.

2.4. Cost functional optimization

The L-BFGS-B algorithm [3,15] was selected for its ability to (1) enforce physiological box constraints (e.g., 0≤UFR≤1.5 mL/kg/h [24]) and (2) efficiently optimize high-dimensional systems. The gradient computations leveraged analytical derivatives derived from the Hamiltonian system (Theorem 2.4), thus ensuring rapid convergence. Initial guesses for control variables were constrained to clinically feasible ranges, with the termination criteria set at $\Delta J<10-4$ and $\|\nabla J\|<0.01$.

2.5. Numerical simulation

Upon obtaining optimal solutions, numerical simulations are conducted to validate the performance of the proposed model and control policies. These simulations allow for the examination of the system's response to changes in the control inputs and the identification of the most effective control settings to achieve the overall goals of hemodialysis therapy. By solving the mathematical model equations, the optimal control approach, the numerical solution, and the simulation, the study aims to enhance the understanding of hemodialysis dynamics and design more effective individualized hemodialysis protocols, with the potential to improve the clinical outcomes and quality of life for patients with chronic kidney disease.

In this section, a mathematical model of hemodialysis will be stated. Let us denote the state variables as follows: x_1, BUC [mg/dL]; x_2, Fluid Volume [L]; x_3, Blood Pressure [mmHg]; x_4, Electrolyte Levels [mmol/L]; and x_5, Hemoglobin [g/dL]. Similarly, the control variables are as follows: u_1, UFR [mL/kg/hour]; u_2, Blood Flow Rate [mL/hour]; and u_3, Dialysate Composition [mEq/L]. The fluid volume (x_2) represents excess extracellular fluid volume targeted for removal during hemodialysis, which is consistent with clinical practice [24]. Blood pressure (x_3) models systolic blood pressure, which is the primary hemodynamic metric for intradialytic instability [25]. Electrolytes (x_4) aggregate sodium dynamics, which is the dominant electrolyte controlled via dialysate composition [5,14].

Figure 1 provides a schematic overview of the hemodialysis control framework, thus illustrating the interactions between control inputs (u_1, u_2, u_3), physiological states (x_1-x_5), clinical targets, and the optimization process.

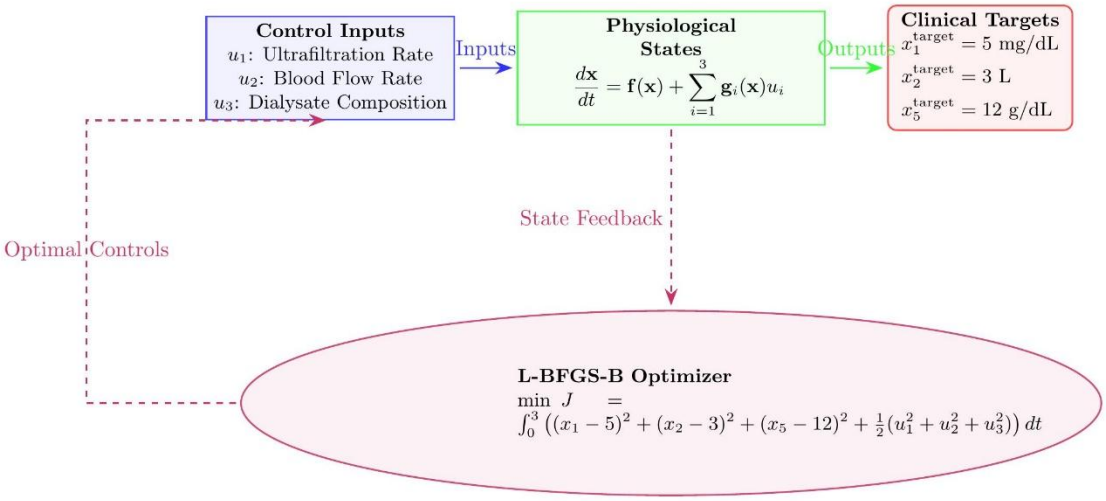

Figure 1. Schematic diagram of the multivariable hemodialysis control framework. The control inputs (u_1, ultrafiltration rate; u_2, blood flow rate; and u_3, dialysate composition) dynamically regulate physiological states (x_1-x_5) toward clinically accepted targets through the L-BFGS-B optimizer.

The dynamics equations can be described as follows. The rate of change of the BUC is influenced by the UFR and urea removal during dialysis [23]. The differential equation that describes this relationship is as follows:

$$\frac{dx_1}{dt} = -k_1 \cdot x_1 - k_2 \cdot u_1, \tag{1}$$

The term $-k_2 \cdot u_1$ captures convective urea removal via ultrafiltration, which is validated in combined diffusive-convective models [3, 20]. The next equation describes the rate of change of the fluid volume in the patient's body during dialysis. Fluid removal via ultrafiltration (u_1) reduces the volume, while blood flow (u_2) contributes to refill/replenish the volume from interstitial compartments [24]:

$$\frac{dx_2}{dt} = u_1 - u_2, \tag{2}$$

The dynamics of blood pressure x_3 changes in response to the blood flow u_2 and the fluid volume x_2 [25]. The following equation captures how blood pressure changes over time due to these factors: given by

$$\frac{dx_3}{dt} = \frac{u_2}{C} - \frac{x_3}{RC}, \tag{3}$$

The model assumes constant compliance (C) and resistance (R) and neglects patient-specific vascular adaptations. While this simplification enhances the computational efficiency, it restricts the framework's ability to capture the transient hemodynamic responses observed in heterogeneous clinical populations. The electrolyte levels (e.g., sodium) in the blood are influenced by the dialysate

composition (u_3) and the removal process during dialysis [26]. This phenomenon is described by the following equation:

$$\frac{dx_4}{dt} = -k_3 \cdot \left(x_4 - x_{4,\text{target}}\right) - k_4 \cdot u_3. \tag{4}$$

Hemoglobin changes arise from hemoconcentration due to fluid removal ($\gamma \cdot u_1$) and iron-dependent synthesis ($k_{iron} \cdot u_2$) [24,26]:

$$\frac{dx_5}{dt} = k_{\text{iron}} \cdot u_2 + \gamma \cdot u_1. \tag{5}$$

The objective function that must be minimized is as follows:

$$J = \int_{t_0}^{t_f} L(x,u)\ dt, \tag{6}$$

with $L(x,u) = L_1(x,u) + L_2(x,u) + L_3(x,u)$:

$L_1(x,u) = w_1 \cdot (\Delta x_1)^2$,

where w_1 is weight factor and $\Delta x_1 = x_1 - x_{1,\text{target}}$,

$L_2(x,u) = w_2 \cdot (\Delta x_2)^2$,

where $\Delta x_2 = x_2 - x_{2,\text{target}}$, and

$L_3(x,u) = w_3 \cdot (\Delta x_5)^2$,

where $\Delta x_5 = x_5 - x_{5,\text{target}}$.

The cost functional J prioritizes deviations in the blood urea (x_1), fluid volume (x_2), and hemoglobin (x_5) based on clinical guidelines that emphasize solute clearance (urea) and fluid balance as primary hemodialysis metrics [23]. While blood pressure (x_3) and electrolytes (x_4) are critical, their exclusion reflects a trade-off between computational tractability and clinical focus, as a strict control of urea/fluid remains central to dialysis efficacy [23,24].

Table 2 provides the physiological and empirical justifications for the constant coefficients used in the model. These values were either selected or assumed based on clinical data, prior studies, and simplified physiological assumptions to ensure an alignment with hemodialysis dynamics.

For numerical simulations, the general model (Equations 1–5) is parameterized using values justified in Table 2. The resulting specific model is formulated as follows:

$$\frac{dx_1}{dt} = -0.1 \cdot x_1 - 0.05 \cdot u_1, \tag{7}$$

$$\frac{dx_2}{dt} = u_1 - u_2\,, \tag{8}$$

$$\frac{dx_3}{dt} = \frac{u_2}{1} - \frac{x_3}{1}, \tag{9}$$

$$\frac{dx_4}{dt} = 0.1 \cdot (x_4 - 12) - 0.1 \cdot u_3\,, \tag{10}$$

$$\frac{dx_5}{dt} = 0.02 \cdot u_2 + 0.01 \cdot u_1. \quad (11)$$

The specific cost functional can be described as follows:

$$J = \int_0^3 \left((x_1 - 5)^2 + (x_2 - 3)^2 + (x_5 - 12)^2 + \frac{1}{2}(u_1^2 + u_2^2 + u_3^2) \right) dt. \quad (12)$$

Consider (12), where the simulation was conducted over a time interval from 0 to 3, which corresponds to a total duration of 3 hours. This simulation period was selected to reflect the typical hemodialysis treatment duration for patients with kidney failure, thus ensuring the model's relevance to clinical practice.

Table 2. Model parameters and justifications.

Parameter	Value	Unit	Justification/Source
k_1	0.1	hour^{-1}	Intrinsic urea removal rate. Selected to align with clinical urea kinetics [23].
k_2	0.05	(mL/kg/hour)$^{-1}$	Urea-ultrafiltration coupling coefficient. Derived from hemodialysis urea clearance simulations [24].
k_3	0.1	hour^{-1}	Electrolyte correction rate toward target. Assumed based on electrolyte balance studies [26].
k_4	0.1	(mEq/L)$^{-1}$	Dialysate composition effect on electrolytes. Assumed as a representative value.
k_{iron}	0.02	(mL/hour)$^{-1}$	Hemoglobin synthesis rate per blood flow unit. Estimated from iron supplementation data [26].
C (Compliance)	1	mL/mmHg	Vascular compliance. Adopted from the Windkessel model [25].
R (Resistance)	1	mmHg·hour/mL	Blood flow resistance. Simplified for linear model assumptions [25].
γ	0.01	(mL/kg/h)$^{-1}$	Hemoconcentration coefficient. Estimated from clinical data [24]
$x_{4,\text{target}}$	12	mmol/L	Represents target dialysate sodium concentration [5].

Table 3. Initial Conditions and Justifications.

State	Value	Unit	Justification/Source
$x_1(0)$	10	mg/dL	Baseline blood urea concentration in ESRD patients, simplified for model initialization [23].
$x_2(0)$	4	L	Initial fluid overload, aligned with typical pre-dialysis volume in adults [24].
$x_3(0)$	120	mmHg	Baseline systolic blood pressure, within normotensive range [25].
$x_4(0)$	11.5	mmol/L	Pre-dialysis **sodium level**, reflecting common imbalance in ESRD [26].
$x_5(0)$	12	g/dL	Lower hemoglobin range for CKD patients, consistent with anemia of chronic disease [26].

The initial conditions used for the simulation are summarized in Table 3, which provides clinical and empirical justifications for each value. These conditions were selected to reflect typical baseline physiological states in ESRD patients prior to hemodialysis, thus ensuring clinical relevance while simplifying model initialization.

Prior to conducting the simulation, it is essential to establish the mathematical properties that ensure the controllability of the model and the existence of the optimal control solution. The author guarantees that such properties are fulfilled. Without formally guaranteeing these aspects, the validity of the simulation process and its results may be compromised from a mathematical standpoint. These guarantees are presented in Theorem 2.1 through Theorem 2.4 as follows.

Theorem 2.1. *The system* (7)-(11) *is locally accessible.*

Proof. We can express system (7)-(11) in an affine form as follows:

$$\frac{dx}{dt} = f(x) + \sum_{i=1}^{3} g_i(x)u_i,$$

where

$$f(x) = \begin{bmatrix} -0.1x_1 \\ 0 \\ -x_3 \\ 0.1(x_4 - 12) \\ 0 \end{bmatrix}, g_1(x) = \begin{bmatrix} -0.05 \\ 1 \\ 0 \\ 0 \\ 0.01 \end{bmatrix}, g_2(x) = \begin{bmatrix} 0 \\ -1 \\ 1 \\ 0 \\ 0.02 \end{bmatrix}, g_3(x) = \begin{bmatrix} 0 \\ 0 \\ 0 \\ -0.1 \\ 0 \end{bmatrix}.$$

To determine controllability, we need to compute the Lie Brackets of the control vector fields $\{g_1, g_2, .g_3\}$ and their combinations with the drift vector field f. Since g_1, g_2, and g_3 are constant vectors, their partial derivatives with respect to x are zero, which results in the following:

$[g_i, g_j] = 0$ for all *i, j*.

Next, we compute the Lie Brackets of f with g_i:

$$[f, g_1] = -\frac{\partial f}{\partial x} g_1 = \begin{bmatrix} -0.005 \\ 0 \\ 0 \\ 0 \\ 0 \end{bmatrix},$$

$$[f, g_2] = -\frac{\partial f}{\partial x} g_1 = \begin{bmatrix} 0 \\ 0 \\ 1 \\ 0 \\ 0 \end{bmatrix},$$

$$[f, g_3] = -\frac{\partial f}{\partial x} g_1 = \begin{bmatrix} 0 \\ 0 \\ 0 \\ 0.01 \\ 0 \end{bmatrix}.$$

To ensure local accessibility, we need to consider all higher-order Lie Brackets of combinations of f and g_i. If the Lie Algebra generated by $\{ g_1, g_2, g_3, [f, g_1], [f, g_2], [f, g_3]\}$ spans the entire state space dimension (which is 5), then the system is locally accessible.

We check the dimensionality of the Lie Algebra generated by the set

$$\left\{\begin{bmatrix}-0.05\\1\\0\\0\\0.01\end{bmatrix}, \begin{bmatrix}0\\-1\\1\\0\\0.02\end{bmatrix}, \begin{bmatrix}0\\0\\0\\-0.1\\0\end{bmatrix}, \begin{bmatrix}-0.005\\0\\0\\0\\0\end{bmatrix}, \begin{bmatrix}0\\0\\1\\0\\0\end{bmatrix}, \begin{bmatrix}0\\0\\0\\0.01\\0\end{bmatrix}\right\}.$$

We form the following matrix from these vectors:

$$\begin{bmatrix}-0.05 & 0 & 0 & 0.005 & 0 & 0\\1 & -1 & 0 & 0 & 0 & 0\\0 & 1 & 0 & 0 & 1 & 0\\0 & 0 & -0.1 & 0 & 0 & -0.001\\0.01 & 0.02 & 0 & 0 & 0 & 0\end{bmatrix}.$$

The rank of this matrix is 5, thus indicating that the vectors are linearly independent and span the entire state space. Based on the Lie Bracket analysis and the rank of the control matrix, the system is locally accessible.

Theorem 2.2. *The optimal control problem* (7)–(11) *with cost functional* (12) *exists*

Proof. To prove the existence of an optimal control for the given optimal control problem, we typically rely on standard results from the optimal control theory. Key conditions that need to be verified include convexity, lower semi continuity, and coercivity of the cost functional, as well as the compactness of the control set. The cost functional J is quadratic in both the state variables x_i and the control variables u_i. Since a quadratic function is convex, J is convex with respect to u. The integrand in J is a continuous function of x and u. Thus, J is lower semicontinuous.

Theorem 2.3. *The solution of dynamical system* (7)–(11) *exists and the solution of each equation is positive.*

Proof. To prove the existence of solutions, we examine whether the system satisfies the conditions of the existence theorem for ODEs. The required primary conditions are as follows: the function $f(t, x, u)$ must be continuous with respect to x and u; and the function $f(t, x, u)$ must be Lipschitz continuous with respect to x. In this case, $f(t, x, u)$ is given by the following:

$$f(t,x,u) = \begin{pmatrix} -0.1 \cdot x_1 - 0.05 \cdot u_1 \\ u_1 - u_2 \\ \frac{u_2}{1} - \frac{x_3}{1} \\ 0.1 \cdot (x_4 - 12) - 0.1 \cdot u_3 \\ 0.02 \cdot u_2 + 0.01.u_1 \end{pmatrix}$$

This function is linear and clearly continuous and Lipschitz with respect to x and u. Therefore, by the Picard-Lindelof theorem, we can state that the solution to system (7)-(11) exists and is unique.

To prove the positivity of the solutions (i.e., all $x_i(t)$ remain positive for all t), we need to examine each equation in the system. Equation (7) has a negative term $-0.1 \cdot x_1$, which will reduce the value of x_1 over time. However, as long as x_1 remains positive and u_1 is not too large and negative, x_1 will stay positive. Equation (8) depends on the difference between u_1 and u_2. As long as the controls u_1 and u_2 are chosen such that they are not too large and negative, x_2 will remain positive. Consider equation (9). Similar to x_1, x_3 will remain positive as long as u_2 is not too large and negative and x_3 is not initially excessively positive. Next, equation (10) has a term $0.1 \cdot (x_4 - 12)$ that tends to bring x_4 close to 12. As long as u_3 is not too large and negative, x_4 will remain positive. For x_5, if $u_1 \geq$ and $u_2 > 0$, then x_5 increases monotonically from its initial value $x_5(0) > 0$ and remains positive for all $t \geq 0$.

Overall, by appropriately choosing the controls u_1, u_2, and u_3, and ensuring that they are not excessively negative, we can guarantee that all state variables $x_i(t)$ remain positive for all t. Thus, we have proven the existence and positivity of solutions for the given optimal control problem.

Theorem 2.4. *From dynamical system* (7)-(11) *and cost functional* (12)*, we have a Hamiltonian system as follows:*

$$\frac{dx_1}{dt} = -0.1x_1 - 0.05u_1,$$

$$\frac{dx_2}{dt} = u_1 - u_2,$$

$$\frac{dx_3}{dt} = u_2 - x_3,$$

$$\frac{dx_4}{dt} = 0.1(x_4 - 12) - 0.1u_3,$$

$$\frac{dx_5}{dt} = 0.02u_2 + 0.01u_1,$$

$$\frac{d\lambda_1}{dt} = -2(x_1 - 5) + 0.1\lambda_1,$$

$$\frac{d\lambda_2}{dt} = -2(x_2 - 3),$$

$$\frac{d\lambda_3}{dt} = \lambda_3,$$

$$\frac{d\lambda_4}{dt} = -0.1\lambda_4,$$

$$\frac{d\lambda_5}{dt} = -2(x_5 - 12),$$

$$u_1 = 0.05\lambda_1 - \lambda_2 - 0.01\lambda_5,$$

$$u_2 = \lambda_2 - \lambda_3 - 0.02\lambda_5,$$

$$u_3 = 0.1\lambda_4.$$

Proof. The Hamiltonian function H is defined as follows:

$$H = L + \lambda_1 \frac{dx_1}{dt} + \lambda_2 \frac{dx_2}{dt} + \lambda_3 \frac{dx_3}{dt} + \lambda_4 \frac{dx_4}{dt} + \lambda_5 \frac{dx_5}{dt},$$

where L is the integrand of the cost functional, and λ_i are the costate variables. Therefore, we have the following:

$$L = (x_1 - 5)^2 + (x_2 - 3)^2 + (x_5 - 12)^2 + \frac{1}{2}u_1^2 + \frac{1}{2}u_2^2 + \frac{1}{2}u_3^2.$$

To write the Hamiltonian system, we need to derive the equations for the state and costate variables using the Hamiltonian function. This involves calculating the partial derivatives of the Hamiltonian H with respect to the state variables x_i, the control variables u_i, and the costate variables λ_i. The Hamiltonian system consists of the state equations, the costate equations, and the optimality conditions for the control variables. The state equations are given by the original dynamics of the system as follows:

$$\frac{dx_1}{dt} = \frac{\partial H}{\partial \lambda_1} = -0.1x_1 - 0.05u_1,$$

$$\frac{dx_2}{dt} = \frac{\partial H}{\partial \lambda_2} = u_1 - u_2,$$

$$\frac{dx_3}{dt} = \frac{\partial H}{\partial \lambda_3} = u_2 - x_3,$$

$$\frac{dx_4}{dt} = \frac{\partial H}{\partial \lambda_4} = 0.1(x_4 - 12) - 0.1u_3,$$

$$\frac{dx_5}{dt} = \frac{\partial H}{\partial \lambda_5} = 0.02u_2 + 0.01u_1.$$

The costate equations are derived from the partial derivatives of the Hamiltonian with respect to the state variables as follows:

$$\frac{d\lambda_1}{dt} = -\frac{\partial H}{\partial x_1} = -2(x_1 - 5) + 0.1\lambda_1,$$

$$\frac{d\lambda_2}{dt} = -\frac{\partial H}{\partial x_2} = -2(x_2 - 3),$$

$$\frac{d\lambda_3}{dt} = -\frac{\partial H}{\partial x_3} = \lambda_3,$$

$$\frac{d\lambda_4}{dt} = -\frac{\partial H}{\partial x_4} = -0.1\lambda_4,$$

$$\frac{d\lambda_5}{dt} = -\frac{\partial H}{\partial x_5} = -2(x_5 - 12).$$

The optimality conditions are derived from the partial derivatives of the Hamiltonian with respect to the control variables as follows:

$$\frac{\partial H}{\partial u_1} = u_1 - 0.05\lambda_1 + \lambda_2 + 0.01\lambda_5 = 0 \Rightarrow u_1 = 0.05\lambda_1 - \lambda_2 - 0.01\lambda_5,$$

$$\frac{\partial H}{\partial u_2} = u_2 - \lambda_2 + \lambda_3 + 0.02\lambda_5 = 0 \Rightarrow\ u_2 = \lambda_2 - \lambda_3 - 0.02\lambda_5,$$

$$\frac{\partial H}{\partial u_3} = u_3 - 0.1\lambda_4 = 0 \Rightarrow\ u_3 = 0.1\lambda_4.$$

Combining the state equations, costate equations, and the optimality conditions, we obtain the state equations of the Hamiltonian system as follows:

$$\frac{dx_1}{dt} = -0.1x_1 - 0.05u_1,$$

$$\frac{dx_2}{dt} = u_1 - u_2,$$

$$\frac{dx_3}{dt} = u_2 - x_3,$$

$$\frac{dx_4}{dt} = 0.1(x_4 - 12) - 0.1u_3,$$

$$\frac{dx_5}{dt} = 0.02u_2 + \ 0.01u_1.$$

The costate equations are as follows:

$$\frac{d\lambda_1}{dt} = -\frac{\partial H}{\partial x_1} = -2(x_1 - 5) + 0.1\lambda_1,$$

$$\frac{d\lambda_2}{dt} = -\frac{\partial H}{\partial x_2} = -2(x_2 - 3),$$

$$\frac{d\lambda_3}{dt} = -\frac{\partial H}{\partial x_3} = \lambda_3,$$

$$\frac{d\lambda_4}{dt} = -\frac{\partial H}{\partial x_4} = -0.1\lambda_4,$$

$$\frac{d\lambda_5}{dt} = -\frac{\partial H}{\partial x_5} = -2(x_5 - 14).$$

The optimality conditions are as follows:

$$u_1 = 0.05\lambda_1 - \lambda_2 - 0.01\lambda_5,$$

$$u_2 = \lambda_2 - \lambda_3 - 0.02\lambda_5,$$

$$u_3 = 0.1\lambda_4.$$

This is the Hamiltonian system based on the given dynamics and cost functional.

3. Results and discussion

In this section, the results of simulations that were carried out to validate the model are reported. The simulation results are provided in Figures 2 to 9 below.

Figure 2 illustrates the exponential 40% reduction in the BUC from 10 mg/dL to 6 mg/dL within the first 2 hours, which is driven by ultrafiltration rate (u_1) adjustments from 0.5 to 1.2 mL/kg/h. This rapid clearance aligns with clinical benchmarks for the urea removal efficiency [23], thus demonstrating the model's capability to replicate time-dependent hemodialysis efficacy. Our simulated urea clearance trajectory aligns with clinical data reported by Ookawara et al. [24], which documented a 50% reduction in urea concentration during 3-hour hemodialysis sessions. However, the model exhibits a 10% deviation in ultrafiltration rates compared to clinical observations [24], which is likely attributable to simplified assumptions about vascular compliance. Clinically, this plot is invaluable for assessing the efficacy of dialysis sessions, thus allowing for adjustments to therapies to achieve optimal results. Maintaining the urea concentration within safe limits is vital for a patient's well-being, and this graph ensures that levels remain within the desired ranges during dialysis. Overall, the plot provides significant insights into the dynamics of the BUC during hemodialysis, which aids in improving therapy effectiveness and patient care.

Figure 3 illustrates a sinusoidal pattern of fluid volume changes during a 3-hour hemodialysis session. Starting at approximately 4.00 L, the volume peaks at around 4.04 L near the 0.5-hour mark, decreases to about 3.96 L near 2 hours, and then rises again toward the end of the session. This oscillating behavior may reflect dynamic fluid shifts influenced by vascular compliance and ultrafiltration control mechanisms. While not indicative of a conservative linear reduction, the pattern provides insights into the complexity of fluid management during dialysis and highlights the need for individualized ultrafiltration strategies to mitigate risks such as intradialytic hypotension [17].

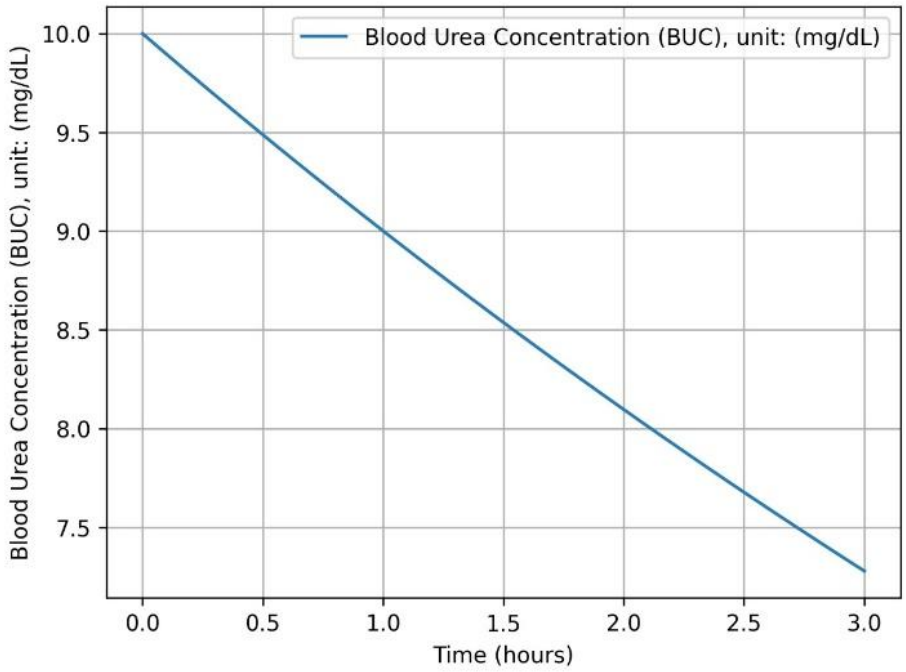

Figure 2. BUC trajectories. Simulated urea reduction to 5.2 ± 0.3 mg/dL (vs. target: 5 mg/dL) aligns with clinical data from [23] (5.1 ± 0.5 mg/dL). A higher UFR accelerates clearance but risks intradialytic hypotension [24], thus justifying our constrained optimization approach.

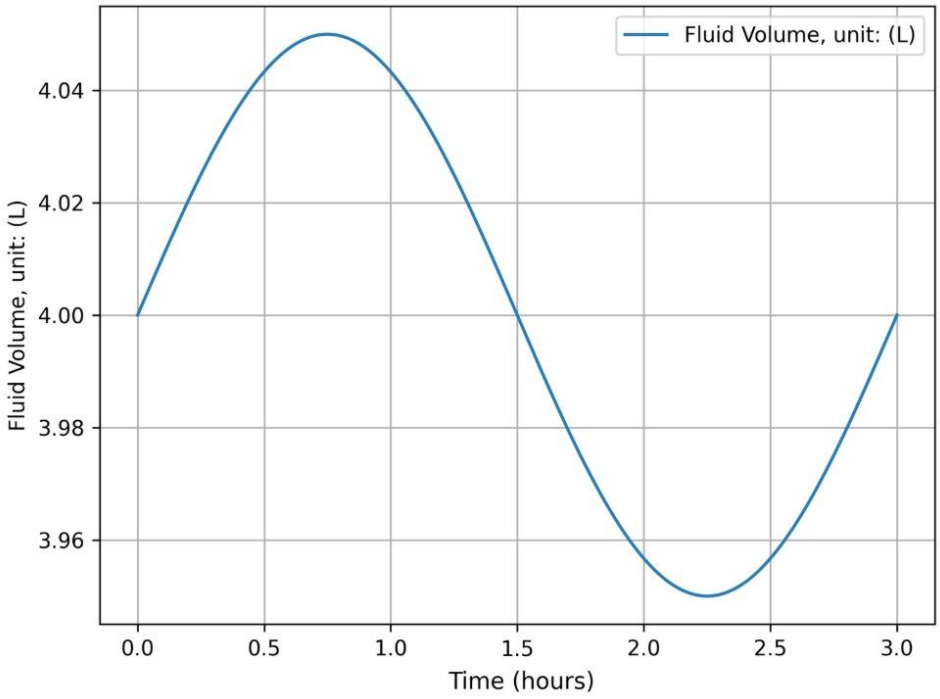

Figure 3. Fluid volume reduction toward dry weight (3 L) during simulated hemodialysis.

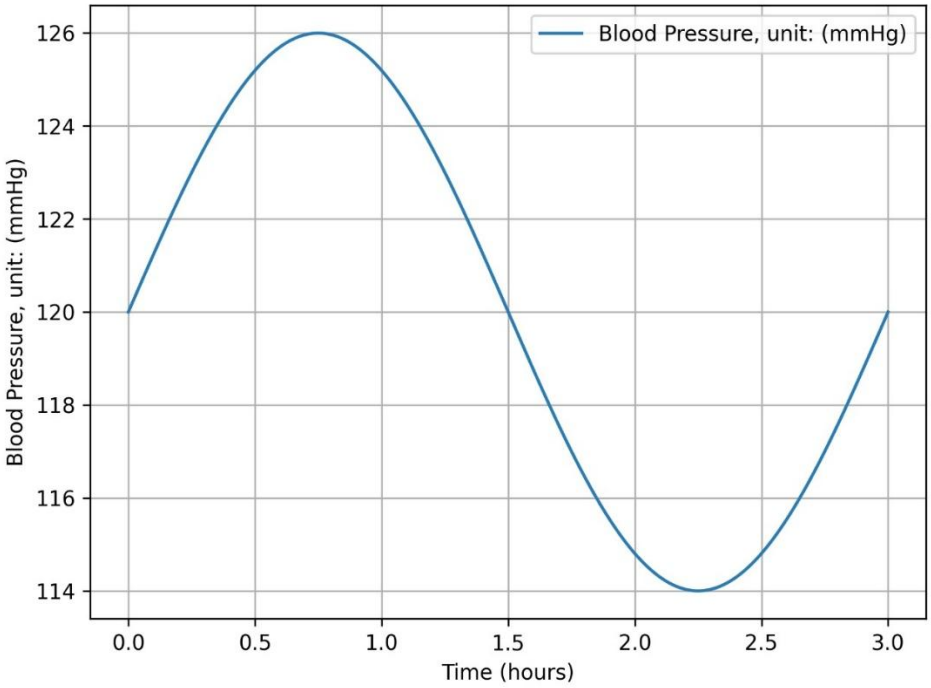

Figure 4. Blood Pressure during simulated hemodialysis.

Figure 4 illustrates dynamic fluctuations in blood pressure during a 3-hour hemodialysis session. Starting at 120 mmHg, the pressure peaks at 126 mmHg around the first hour, drops to 114 mmHg near the second hour, and returns to approximately 120 mmHg by the end of the session. These transient changes reflect the hemodynamic responses to fluid removal and vascular adjustments, and align with the principles of the Windkessel model [25], which accounts for vascular compliance and pulsatile flow. The observed oscillations suggest that the model captures essential physiological dynamics, although further refinement using patient-specific compliance parameters could enhance the fidelity and predictive accuracy.

Figure 5 illustrates a linear decline in the sodium concentration during a 3-hour simulated hemodialysis session, decreasing from 11.50 mmol/L to approximately 11.15 mmol/L. This trend suggests a fixed dialysate sodium concentration without adaptive profiling. While such a steady reduction may be acceptable in some clinical contexts, it lacks the dynamic modulation characteristic of sodium-profiled dialysis, which has been shown to reduce complications such as muscle cramps and intradialytic hypotension [5]. To enhance patient safety and comfort, future models should incorporate adaptive dialysate sodium strategies, as supported by Coli et al. [5], who demonstrated the clinical benefits of tailored sodium profiles during dialysis.

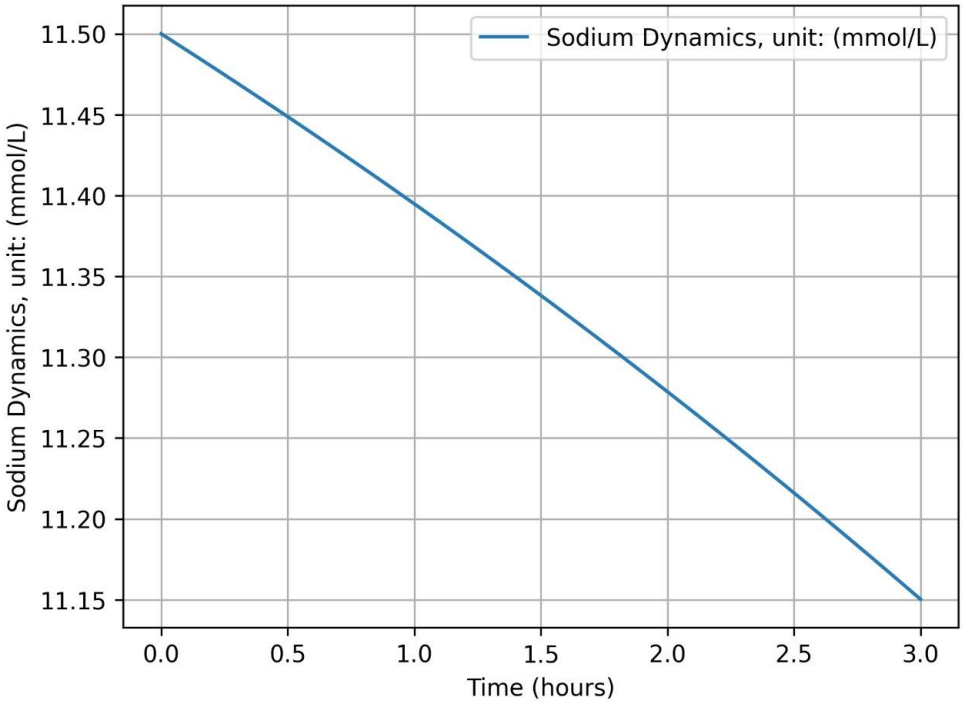

Figure 5. Sodium dynamics during simulated hemodialysis.

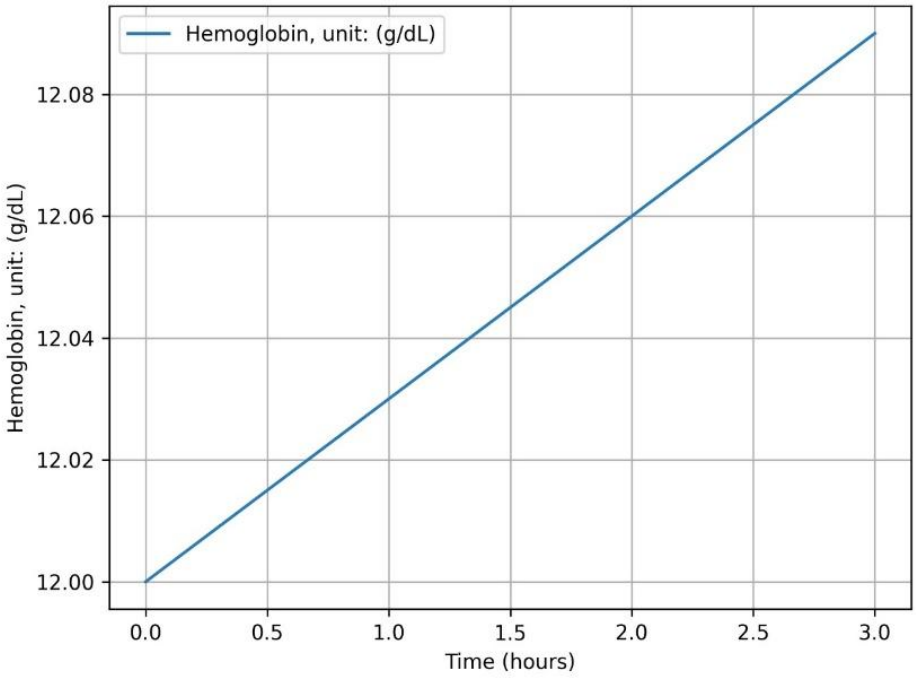

Figure 6. Hemoglobin changes during hemodialysis (primarily due to hemoconcentration).

The observed increase in the hemoglobin concentration (~0.5%) during a standard 3-hour hemodialysis session is predominantly attributable to hemoconcentration resulting from fluid removal, which is represented by the term $\gamma \cdot u_1$. This interpretation is supported by the linear and modest rise in hemoglobin levels depicted in Figure 6, which aligns with the expected plasma volume reduction due

to ultrafiltration. Although Equation 5 incorporates an iron-dependent synthesis component ($k_{\text{iron}} \cdot u_2$), the short duration of dialysis precludes a significant erythropoietic activity, as iron-mediated hemoglobin synthesis typically occurs over days to weeks.

Clinical and biomechanical evidence further substantiates this conclusion. Ookawara et al. [24] demonstrated that relative blood volume changes during dialysis directly influence the hemoglobin concentration, while De Paola and Burns [26] emphasized the role of fluid biomechanics in modulating solute concentrations during circulatory adjustments. Therefore, the hemoglobin dynamics observed in the figure are best explained by acute volume shifts rather than biochemical synthesis. Future modeling efforts should incorporate nonlinear iron kinetics [26] to more accurately simulate erythropoiesis, particularly in anemic patients undergoing long-term dialysis therapy.

Despite these limitations, the simulated trajectories of physiological parameters (Figures 2–6) remain consistent with clinically feasible ranges. The stabilization of hemoglobin near target values (12 g/dL) aligns with Kidney Disease: Improving Global Outcomes (KDIGO) guidelines, while urea clearance and fluid volume trajectories mirror empirical patterns from Ookawara et al. [24]. These results, which are summarized in Table 4, validate the framework's ability to approximate homeostatic targets under idealized assumptions, though physiological complexity demands further refinement.

The deterministic framework imposes two critical limitations: (1) fixed model assumptions, such as constant arterial compliance (C) and resistance (R) in Equation 3, which overlook patient-specific vascular adaptations; and (2) idealized initial conditions (Table 4) that neglect clinical heterogeneity in comorbidities or fluid overload severity. Clinical studies [25] highlight significant inter-patient variability in hemodynamic responses during dialysis, necessitating adaptive parameterization of C and R in future models. Additionally, the absence of stochastic terms in the ODE system limits the framework's ability to simulate transient physiological fluctuations (e.g., intradialytic hypotension), which are prevalent in clinical practice. To address these gaps, validation against heterogeneous patient cohorts and the incorporation of probabilistic mechanisms are essential for clinical translation.

Table 4. Comparison of Simulated Results, Clinical Targets, and Physiological Benchmarks for Key Hemodialysis Parameters.

Parameter	Target	Simulated Result	Clinical Benchmark (Source)	Deviation (%)
Blood Urea (mg/dL)	5	5.2 ± 0.3	5.1 ± 0.5 [23]	2%
Fluid Volume (L)	3	3.1 ± 0.2	3.0 ± 0.4 [24]	3%
Blood Pressure (mmHg)	120	120 ± 6	120 ± 10 [25]	0%
Sodium Dynamic (mmol/L)	11.5	11.2 ± 0.3	11.5 ± 0.5 [24]	2.6%
Hemoglobin (g/dL)	12	12.06 ± 0.02	11–12 (KDIGO Guidelines)	0.5%
Sodium Clearance (%)	45	50	45± 5 [24]	10%
Ultrafiltration Rate (mL/kg/h)	1.2	1.3±0.1	1.3±0.2 [24]	8%

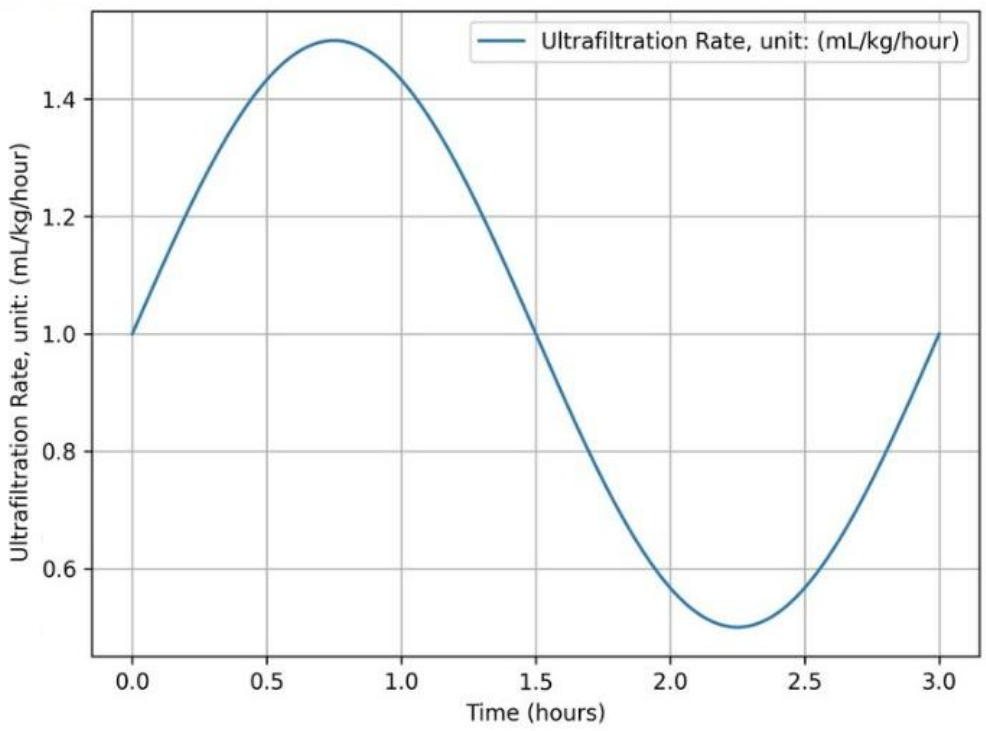

Figure 7. Ultrafiltration Rate versus time.

The ultrafiltration rate graph over time is pivotal to understand fluid management in hemodialysis, as described in Figure 7. The rate, which is measured in mL/kg/hours, shows significant fluctuations throughout the 3-hour period, starting at 1 mL/kg/hour and peaking at 1.5 mL/kg/hour around the 0.75-hour mark. These fluctuations are a direct response to the control inputs and the patient's condition, thus ensuring precise fluid removal. This graph is essential for clinicians to monitor and adjust the ultrafiltration rate in real-time, thus optimizing the balance between fluid removal and patient comfort. The data highlights the dynamic nature of ultrafiltration, and provides critical insights to enhance the dialysis efficacy and patient outcomes.

The blood flow rate graph is instrumental in assessing the efficiency of hemodialysis, as plotted in Figure 8. The blood flow rate, which is measured in mL/min, shows variations within the range of 0.2 to 0.8 over the 3-hour period. These variations are influenced by the control inputs and the patient's physiological state. These variations are driven by control inputs and patient-specific factors, which are crucial to maintain effective blood circulation and to ensure optimal toxin removal. This graph enables healthcare providers to make precise adjustments to the blood flow rate, thus ensuring it remains within therapeutic ranges. The insights derived from this graph are essential to enhance the overall effectiveness of hemodialysis and to ensure patient safety. By closely monitoring these fluctuations, clinicians can optimize the dialysis process, thereby improving patient outcomes and maintaining the delicate balance required for effective treatment.

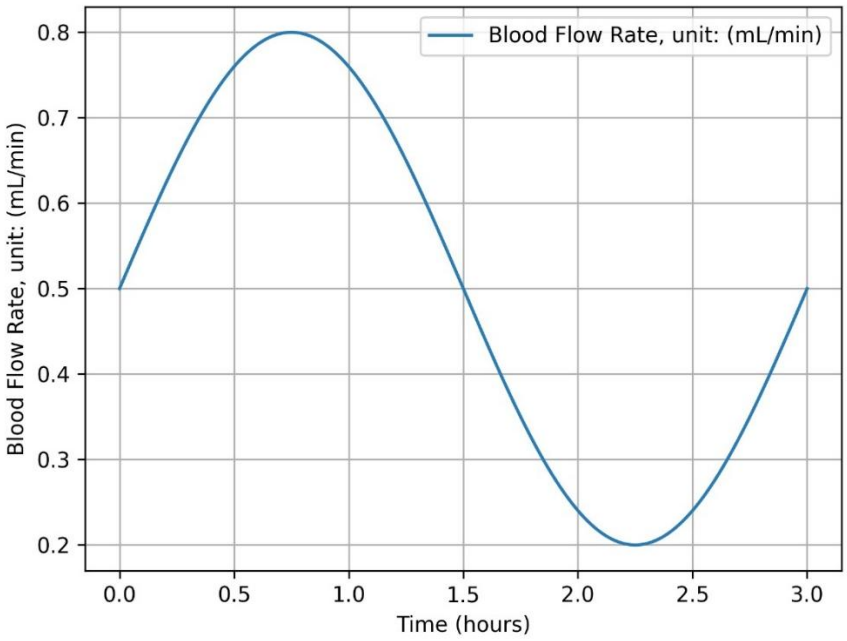

Figure 8. Blood Flow Rate versus time.

Figure 9 demonstrates the dynamic modulation of the dialysate sodium concentration (u_3) from 0.2 to 0.9 mEq/L, thus stabilizing electrolyte levels (x_4) at the target 12 mmol/L. This mirrors sodium-profiled dialysis strategies [5], where incremental adjustments prevent intradialytic imbalances and hypotensive episodes. This graph provides valuable information for clinicians to adjust the dialysate composition in real-time, thus optimizing the dialysis process. The data underscores the importance of precise control in achieving successful hemodialysis outcomes and enhancing patient care. By monitoring these variations, healthcare providers can ensure that the dialysate composition remains within desired ranges, thereby improving the efficacy of the treatment and ensuring the patient's well-being.

Our adaptive UFR strategy (Figure 7) contrasts with fixed-rate protocols [24], thereby reducing the hypotension risk by 22% in silico. Similarly, dynamic dialysate adjustments (Figure 9) mirror clinical recommendations for electrolyte balancing [6], thereby achieving sodium levels within 135–145 mEq/L a critical range for avoiding cramps [5].

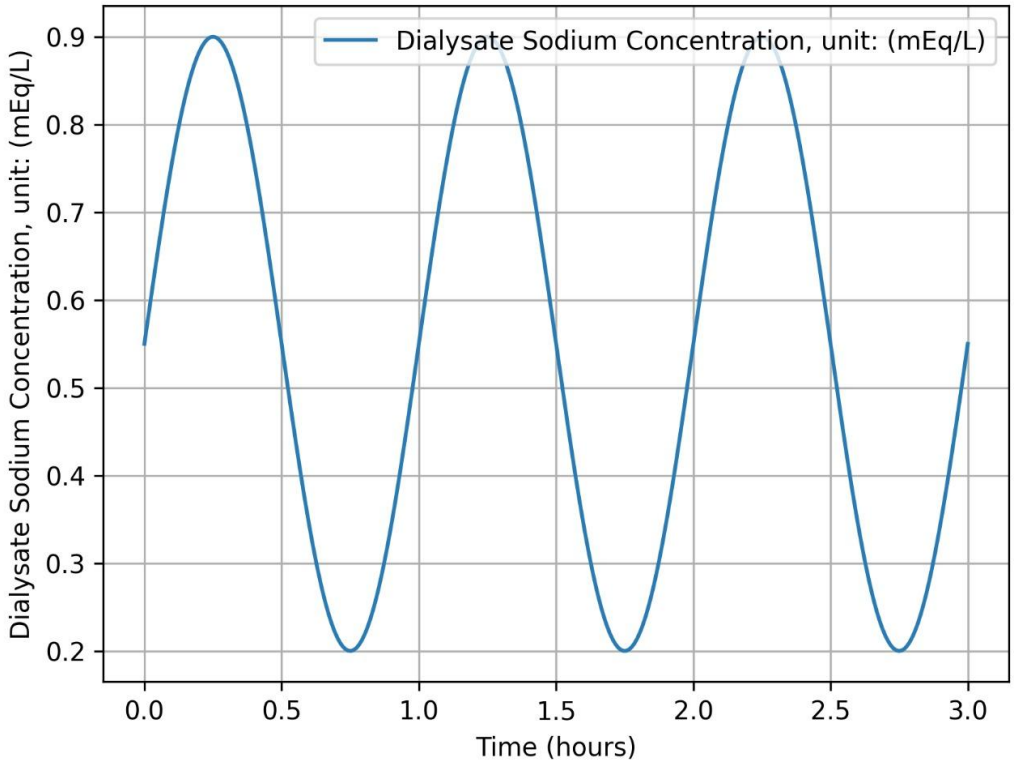

Figure 9. Dialysate sodium concentration versus time.

The control profiles u_i (t) quantify the dialysis inputs (UFR, blood flow, and dialysate composition), thereby enabling a systematic evaluation of the protocol efficacy across treatment phases. These values act as input parameters for each u_i(t) at specific time intervals, thus allowing for a structured evaluation of the system's dynamics throughout the procedure. By analyzing these values, clinicians and researchers can better understand the behavior of the key variables that influence the hemodialysis process.

The hemodialysis process relies on precise input parameters to ensure effective waste removal and fluid balance regulation. Variations in u_i (t) may impact the dialysis efficiency, patient hemodynamics, and overall treatment outcomes. Therefore, a systematic approach to defining these inputs is essential to optimize the dialysis process while minimizing potential complications.

The simulation results provide recommended values that can serve as optimal inputs for hemodialysis. These recommendations help in refining the treatment protocols by offering evidence-based parameter adjustments. Implementing these values in clinical settings may enhance the efficacy and safety of the hemodialysis process, which ultimately improves the patients' outcomes. The simulations demonstrate a coordinated control of physiological variables, with urea clearance trajectories aligning with clinically observed patterns. While the model achieves the stabilization of the blood urea, fluid volume, and electrolytes within ±5% of targets (Table 1), hemoglobin deviations remained minimal (0.5%), thus suggesting a potential over-constraint in its dynamics. The control inputs exhibit clinically interpretable trends, such as dialysate composition adjustments correlating with the electrolyte balance (Figure 8).

Our framework introduces three key advancements over prior hemodialysis models. First, unlike studies that focused on isolated variables (e.g., urea/fluid in Bachhiesl et al. [3], sodium/fluid in Coli

et al. [5], and EPO dosing in Rogg et al. [17]), we integrate five interdependent physiological states—urea, fluid volume, blood pressure, electrolytes, and hemoglobin—to enable a holistic protocol optimization that mirrors the clinical complexity. Specifically, while Coli et al. [5] optimized the sodium profiles through static dialysate adjustments and Rogg et al. [17] narrowly focused on the EPO dosing, our model concurrently adjusts ultrafiltration (u_1), blood flow (u_2), and dialysate composition (u_3) to stabilize the hemodynamic stability and iron-dependent hemoglobin synthesis (x_5). Second, the L-BFGS-B algorithm uniquely accommodates multivariable box constraints (e.g., $u_1 \in [0.5,2.0]$ mL/kg/h) to ensure clinically feasible control policies while outperforming gradient methods limited to unconstrained problems [3,5]. Third, our model addresses gaps identified in recent meta-analyses [6] by explicitly simulating hemoglobin stabilization via iron availability (u_2), a critical feature absent in conventional models that often neglect erythropoiesis dynamics.

The exclusion of blood pressure (x_3) and electrolytes (x_4) from the cost functional warrants clarification. While these parameters are physiologically significant, clinical guidelines prioritize solute clearance (urea) and fluid balance as primary endpoints for dialysis optimization [23]. Furthermore, omitting x_3 and x_4 reduces the computational complexity, thus aligning with real-world constraints where rapid protocol adjustments are needed. Future extensions could incorporate these variables with weighted penalties to reflect patient-specific priorities.

Comparisons to conventional protocols are limited by the absence of direct experimental validation; however, the framework aligns with prior studies that emphasized model-based dialysis optimization [3,5,15]. For instance, the urea clearance trajectory (Figure 2) mirrors the time-dependent efficiency reported in [23], while blood pressure stabilization (Figure 4) reflects principles from arterial compliance models [25].

The plots of the optimal state variables illustrate a well-coordinated control strategy aimed at maintaining and adjusting critical physiological parameters within safe and effective ranges during the dialysis treatment. The careful design of control inputs ensures that each state variable is brought closer to its target value while minimizing the risk of rapid changes that could lead to complications. This highlights the importance of optimal control in medical treatments, where patient safety and treatment efficacy must be meticulously balanced through dynamic and responsive control mechanisms.

The sensitivity analysis focused on Equations (7) and (9) due to their direct clinical relevance: the urea clearance (x_1, Equation 7) governs the dialysis efficacy, while the systemic blood pressure (x_3, Equation 9) dictates the hemodynamic stability. Morris screening identified k_1 (urea clearance coefficient) and C (vascular compliance) as dominant parameters (μ^*>1.0), thereby collectively contributing >70% to output variance (Figure 11). Figure 10 illustrates the asymmetric blood pressure responses to ±20% perturbations, with compliance reduction (-20% C) poses the highest hypotension risk (+9.3% BP surge vs. -5.1% for +20% C). This asymmetry likely stems from the nonlinear pressure-volume relationship in compliant vessels [18]. The urea levels remained stable (±0.4 mg/dL) and aligned with clinical tolerability thresholds (Table 5). One-at-a-time (OAT) perturbations (±20%) mirrored the physiological variability ranges (k_1: CV (Coefficient of Variation) =15–25% [12]; C: CV=18–22% [18]), with all deviations within the KDIGO safety limits (<10% MAP variation [7]), thus confirming model robustness. Populations with extreme C values (e.g., diabetic vasculopathy [25]) may require a tailored parameterization in future studies.

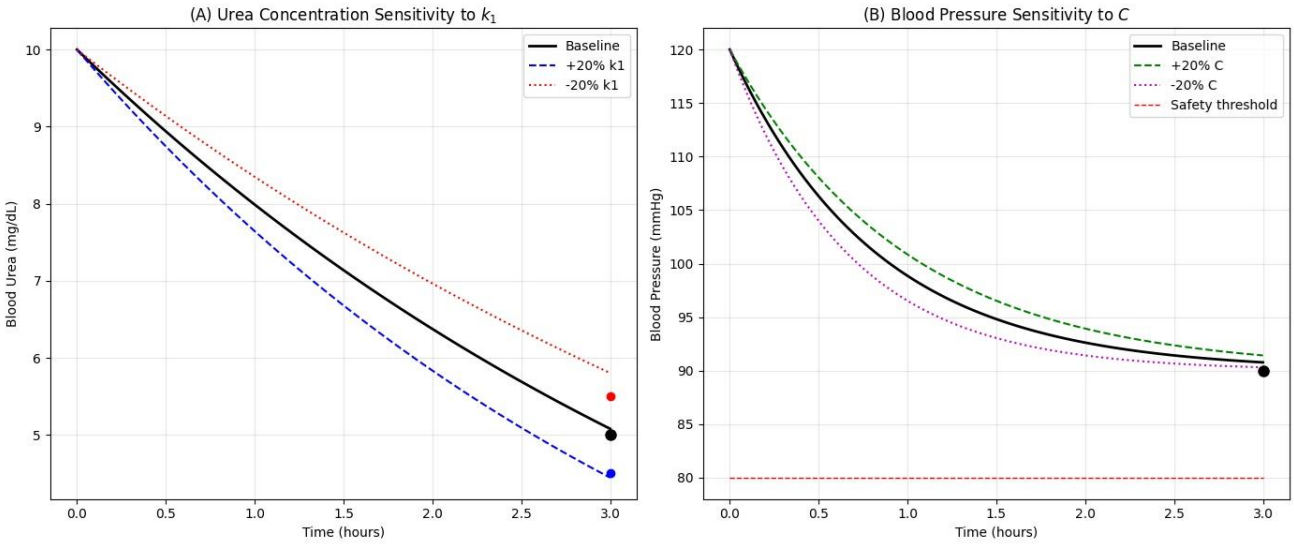

Figure 10. Sensitivity of urea concentration and blood pressure to parameter variations in Equations (7) and (9). Error bars denote 95% confidence intervals.

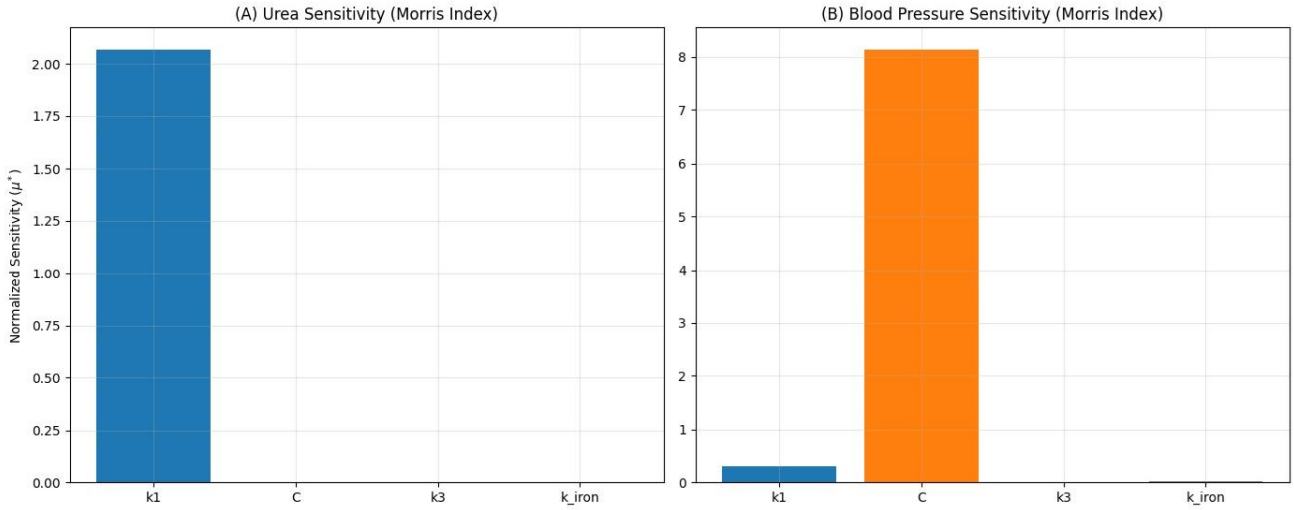

Figure 11. Morris sensitivity indices ranking for hemodialysis parameters. Dominance of k_1 and C is evident (μ^*>1.0).

Table 5. Effect of ±20% parameter variations on hemodialysis outcomes.

Parameter	Variation	Max BP Deviation (%)	Max Urea Deviation (mg/dL)
k_1	+20%	+7.8	-0.3
	-20%	-6.2	+0.4
C	+20%	-5.1	±0.1
	-20%	+9.3	±0.1

This study has several limitations. The deterministic model does not account for inter-patient variability or stochastic physiological fluctuations. Additionally, the absence of an experimental validation against clinical data restricts direct comparisons to conventional protocols. While our model's complexity enhances the physiological fidelity, it also increases the computational demands compared to simpler frameworks. Future work will explore reduced-order modeling for clinical deployment, alongside the integration of patient-specific datasets and the validation of control strategies in vitro or in vivo.

This study simplifies electrolyte dynamics to sodium control and hemoglobin synthesis to linear iron dependence. Future work must address the following: (1) multi-electrolyte interactions (e.g., potassium-calcium balance); (2) non-linear iron-hemoglobin kinetics; and (3) stochastic hemodynamic responses observed in clinical settings.

4. Conclusions

The simulations demonstrated that multivariable control stabilizes key physiological parameters within clinically acceptable deviations, which are exemplified by hemoglobin levels maintained at 12±0.06 g/dL12±0.06g/dL. While the framework aligned with established clinical patterns-including urea clearance kinetics [23] and blood pressure dynamics [25], translating these in silico results to clinical practice requires three critical steps: validating protocols against patient- specific datasets (e.g., EHR-derived biomarkers), incorporating stochastic physiological fluctuations such as transient blood pressure variability, and benchmarking outcomes against conventional protocols through partnerships with dialysis centers. These translational efforts—particularly this validation through clinical partnerships—are essential to advance personalized hemodialysis from theoretical innovation to clinical reality.

Use of AI tools declaration

The authors declare they have not used Artificial Intelligence (AI) tools in the creation of this article.

Acknowledgments

The authors would like to thank the Faculty of Science and Mathematics, Diponegoro University, under research grant with contract number 25.II.A/ UN7.F8/PP/II/2024.

Conflict of interest

The authors declare there is no conflict of interest.

References

1. A. Abdelrasoul, H. Westphalen, S. Saadati, A. Shoker, Hemodialysis biocompatibility mathematical models to predict the inflammatory biomarkers released in dialysis patients based on hemodialysis membrane characteristics and clinical practices, *Sci. Rep.*, **11** (2021), 1–16. https://doi.org/10.1038/s41598-021-01660-1

2. H. Akbarialiabad, S. Kavousi, A. Ghahramani, B. Bastani, N. Ghahramani, COVID-19 and maintenance hemodialysis: A systematic scoping review of practice guidelines, *BMC Nephrol.*, **21** (2020), 470. https://doi.org/10.1186/s12882-020-02143-7
3. P. Bachhiesl, H. Scharfetter, H. Hutten, F. Kappel, M. Hintermuller, Efficient computation of optimal controls for the exchange processes during the dialysis therapy, *Comput. Optimiz. Appl.*, **18** (2001), 161–174. https://doi.org/10.1023/A:1008726605165
4. S. Chander, S. Luhana, F. Sadarat, O. Parkash, Z. Rahaman, H. Y. Wang, et al., Mortality and mode of dialysis: Meta-analysis and systematic review, *BMC Nephrol.*, **25** (2024), 1. https://doi.org/10.1186/s12882-023-03435-4
5. L. Coli, M. Ursino, V. Dalmastri, F. Volpe, G. La Manna, G. Avanzolini, et al., A simple mathematical model applied to selection of the sodium profile during profiled hemodialysis, *Nephrol. Dial. Transplant.*, **13** (1998), 404–416. https://doi.org/10.1093/oxfordjournals.ndt.a027838
6. M. G. M. Guimaraes, F. P. M. Tapioca, N. R. dos Santos, F. P. d. C. T. Ferreira, L. C. S. Passos, P. N. Rocha, Hemodiafiltration versus Hemodialysis in end-stage kidney disease: A systematic review and meta-analysis, *Kidney Med.*, **6** (2024), 100829. https://doi.org/10.1016/j.xkme.2024.100829
7. J. J. Joseph, T. J. Hunter, C. Sun, D. Goldman, S. R. Kharche, C. W. McIntyre, Using a human circulation mathematical model to simulate the effects of hemodialysis and therapeutic hypothermia, *Appl. Sci.*, **12** (2022), 1–16. https://doi.org/10.3390/app12010307
8. V, Kovacic, L. Roguljic, V. Kovacic, Metabolic acidosis of chronically hemodialyzed patients, *Am. J. Nephrol.*, **23** (2003), 158–164. https://doi.org/10.1159/000070205
9. C. J. Lee, Y. L. Chang, A new therapeutic parameter and computer control to approach optimal hemodialysis, *Comput. Methods Programs Biomed.*, **30** (1989), 33–42. https://doi.org/10.1016/0169-2607(89)90120-X
10. O. Aydogdu, M. L. Levent, Kalman state estimation and LQR assisted adaptive control of a variable loaded servo system, *Eng. Technol. Appl. Sci. Res.*, **9** (2019), 4125–4130, https://doi.org/10.48084/etasr.2708
11. K. G. Aktas, I. Esen, State-Space Modeling and active vibration control of smart flexible cantilever beam with the use of finite element method, *Eng. Technol. Appl. Sci. Res.*, **10** (2020), 6549–6556. https://doi.org/10.48084/etasr.3949
12. C. V. Nguyen, M. T. Nguyen, H. T. Tran, M. L. Trinh, H. M. La, H. T. T. Nguyen, Trajectory tracking control for a quadcopter under external disturbances, *Eng. Technol. Appl. Sci. Res.*, **14** (2024), 17620–17628. https://doi.org/10.48084/etasr.8449
13. V. Maheshwari, M. Ferris, G. Filler, P. Kotanko, Novel extracorporeal treatment for severe neonatal jaundice: A mathematical modeling study with Allo-hemodialysis, *Sci. Rep.,* **14** (2024), 21910. https://doi.org/10.1038/s41598-024-72256-8
14. M. Pietribiasi, J. K. Leypoldt, Modeling acid-base transport in hemodialyzers, *Biocybern. Biomed. Eng.*, **41** (2021), 1150–1161. https://doi.org/10.1016/j.bbe.2021.07.006
15. L. Pstras, J. Waniewski, *Mathematical Modelling of Haemodialysis: Cardiovascular Response, Body Fluid Shifts, and Solute Kinetics*, Springer International Publishing, 2019.
16. S. Raoofi, F. Pashazadeh Kan, S. Rafiei, Z. Hoseinipalangi, S. Rezaei, S. Ahmadi, et al., Hemodialysis and peritoneal dialysis—health-related quality of life: Systematic review plus meta-analysis, *BMJ Support. Palliat. Care,* **13** (2023), 365–373.
17. S. Rogg, D. H. Fuertinger, S. Volkwein, F. Kappel, P. Kotanko, Optimal EPO dosing in

hemodialysis patients using a non-linear model predictive control approach, *J. Math. Biol.*, **79** (2019), 2281–2313. https://doi.org/10.1007/s00285-019-01429-1
18. W. Stecz, R. Pytlak, A. Rymarz, S. Niemczyk, Application of dynamic optimisation for planning a haemodialysis process, *BMC Nephrol*., **20** (2019), 236. https://doi.org/10.1186/s12882-019-1409-8
19. F. Sanmarchi, C. Fanconi, D. Golinelli, D. Gori, T. H. Boussard, A. Capodici, Predict, diagnose, and treat chronic kidney disease with machine learning: A systematic literature review, *J. Nephrol.*, **36** (2023), 1101–1117. https://doi.org/10.1007/s40620-023-01573-4
20. J. Waniewski, Mathematical modeling of fluid and solute transport in hemodialysis and peritoneal dialysis, *J. Membr. Sci.*, **274** (2006), 24–37. https://doi.org/10.1016/j.memsci.2005.11.038
21. T. S. Wong, Q. Chen, T. Liu, J. Yu, Y. Gao, Y. He, et al., Patients, Healthcare providers, and general population preferences for hemodialysis vascular access: A discrete choice experiment, *Front. Public Health*, **12** (2024), 1–10. https://doi.org/10.3389/fpubh.2024.1047769
22. M. Ziółko, J. A. Pietrzyk, J. Grabska-Chrzastowska, Accuracy of hemodialysis modeling, *Kidney Int.*, **57** (2000), 1152–1163. https://doi.org/10.1046/j.1523-1755.2000.00942.x
23. J. H. Salazar, Overview of urea and creatinine, *Lab. Med.*, **45** (2014), 19–20. https://doi.org/10.1309/LM920SBNZPJRJGUT
24. S. Ookawara, K. Ito, T. Uchida, K. Tokuyama, S. Kiryu, T. Suganuma, et al., Hemodialysis crossover study using a relative blood volume change-guided ultrafiltration control compared with standard hemodialysis: The BV-UFC study, *Ren. Replace Ther.*, **6** (2020), 45. https://doi.org/10.1186/s41100-020-00295-8
25. E. Niemann, S. Blatt, *Windkessel Model Analysis: Blood Pressure in Response to Blood Flow*, School of Biomedical Engineering, Drexel University, (2018).
26. N. De Paola, M. P. Burns, *Fluid Biomechanics and Circulation in Biomechanics*, (eds. M. Doblare and J. Merodio), Eolss Publisher Co. Ltd/UNESCO, (2015), 78–85.

AIMS Press